Continental Shelf Research 72 (2014) 107–118

Contents lists available at ScienceDirect

Continental Shelf Research

journal homepage: www.elsevier.com/locate/csr

Research papers

A water column study of methane around gas flares located at the West Spitsbergen continental margin ☆

Torben Gentz [a,*], Ellen Damm [a], Jens Schneider von Deimling [b], Susan Mau [a], Daniel Frank McGinnis [c,d], Michael Schlüter [a]

[a] Alfred Wegener Institute for Polar and Marine Research (AWI), Am Handelshafen 12, D-27570 Bremerhaven, Germany
[b] Helmholtz Centre for Ocean Research (GEOMAR), Wischhofstr. 1-3, D-24148 Kiel, Germany
[c] Department of Experimental Limnology, Leibniz Institute of Freshwater Ecology and Inland Fisheries (IGB), Alte Fischerhuette 2, 16775 Stechlin, Germany
[d] Nordic Center for Earth Evolution (NordCEE), Institute of Biology, University of Southern Denmark, 5230 Odense M, Denmark

ARTICLE INFO

Article history:
Received 2 January 2013
Received in revised form
26 July 2013
Accepted 31 July 2013
Available online 16 August 2013

Keywords:
Methane pathways
Gas bubbles
Under water mass spectrometry
Oxidation rates
Isotopic ratio
Gas hydrate

ABSTRACT

In the Arctic Seas, the West Spitsbergen continental margin represents a prominent methane seep area. In this area, free gas formation and gas ebullition as a consequence of hydrate dissociation due to global warming are currently under debate. Recent studies revealed shallow gas accumulation and ebullition of methane into the water column at more than 250 sites in an area of 665 km^2. We conducted a detailed study of a subregion of this area, which covers an active gas ebullition area of 175 km^2 characterized by 10 gas flares reaching from the seafloor at ~245 m up to 50 m water depth to identify the fate of the released gas due to dissolution of methane from gas bubbles and subsequent mixing, transport and microbial oxidation.

The oceanographic data indicated a salinity-controlled pycnocline situated ~20 m above the seafloor. A high resolution sampling program at the pycnocline at the active gas ebullition flare area revealed that the methane concentration gradient is strongly controlled by the pycnocline. While high methane concentrations of up to 524 nmol L^{-1} were measured below the pycnocline, low methane concentrations of less than 20 nmol L^{-1} were observed in the water column above. Variations in the $\delta^{13}C_{CH_4}$ values point to a ^{13}C depleted methane source (~ −60‰ VPDB) being mainly mixed with a background values of the ambient water (~ −37.5‰ VPDB). A gas bubble dissolution model indicates that ~80% of the methane released from gas bubbles into the ambient water takes place below the pycnocline. This dissolved methane will be laterally transported with the current northwards and most likely microbially oxidized in between 50 and 100 days, since microbial CH_4 oxidation rates of 0.78 nmol d^{-1} were measured. Above the pycnocline, methane concentrations decrease to local background concentration of ~10 nmol L^{-1}.

Our results suggest that the methane dissolved from gas bubbles is efficiently trapped below the pycnocline and thus limits the methane concentration in surface water and the air–sea exchange during summer stratification. During winter the lateral stratification breaks down and fractions of the bottom water enriched in methane may be vertically mixed and thus be potentially an additional source for atmospheric methane.

1. Introduction

Methane (CH_4) is the most abundant organic compound in the atmosphere and is influencing the global climate. This greenhouse gas has a global warming potential that is 20–40 times higher than that of carbon dioxide (CO_2) on a 100 year timescale, and CH_4 emissions constitute the second largest contribution to historical warming after CO_2 (Shindell et al., 2009). Present estimates, compiled in the IPCC report (2007), reveal an emission of 503–610 Tg CH_4 yr^{-1} entering the atmosphere. Geological sources, such as micro seepages, geothermal seeps, mud volcanoes or pockmarks have an additional emission potential of 40–60 Tg CH_4 yr^{-1} (Etiope, 2004; Etiope and Klusman, 2002; Kvenvolden and Rogers, 2005). This includes the emission from seabed methane release in marine environments (Kvenvolden and Rogers, 2005) which occurs worldwide on continental margins, estuaries, and river deltas (Judd and Hovland, 2007). Prominent locations are the Håkon Mosby Mud Volcano (Felden et al., 2010; Jerosch et al.,

* Corresponding author. Tel.: +49 471 4831 2029; fax: +49 471 4831 1425.
E-mail address: torben.gentz@awi.de (T. Gentz).

0278-4343/$ - see front matter © 2013 The Authors. Published by Elsevier Ltd. All rights reserved.
http://dx.doi.org/10.1016/j.csr.2013.07.013

2007; Sauter et al., 2006), the Tommeliten and Gullfaks fields in the North Sea (Hovland, 2007; Hovland and Sommerville, 1985; Schneider von Deimling et al., 2011), the Santa Barbara Basin (Fischer, 1978; Leifer and Clark, 2002), the Black Sea (Limonov et al., 1997) as well as the West Spitsbergen continental margin (Hustoft et al., 2009; Knies et al., 2004; Mienert et al., 2005; Westbrook et al., 2008). The emission of CH_4 from marine seeps to the upper water column is estimated to be about 30 Tg CH_4 yr^{-1}, but only 10 Tg CH_4 yr^{-1} might reach the atmosphere (Kvenvolden and Rogers, 2005). The remainder is dissolved and microbially oxidized to CO_2 in the water column (Kvenvolden and Rogers, 2005). However, in shallow shelf areas like the North Sea, the release of CH_4 from the seafloor has a greater potential to enter the atmosphere (Hovland et al., 1993; McGinnis et al., 2006) especially during the well mixed winter season (Schneider von Deimling et al., 2011).

Due to ocean warming, increasing bottom water temperature could result in sub-sea thawing of permafrost (Shakhova et al., 2010) and destabilization of gas hydrates (Jung and Vogt, 2004; Mienert et al., 2005) especially in the Nordic Seas and the Arctic. As a result, Buffett and Archer (2004) estimated an additional release of CH_4 up to tens of Tg yr^{-1} into the water column potentially causing ocean acidification (Biastoch et al., 2011). One of these affected areas could be the West Spitsbergen continental margin investigated in this study (Fig. 1). Previous investigations in this area (e.g., Westbrook et al., 2009) showed a significant release of gas bubbles at more than 250 sites in a water depth between 150 and 400 m striking along a morphological lineation on the seafloor. The release of gas bubbles was detected within and outside the present upper limit of the gas hydrate stability zone (GHSZ), which was detected to be at ~400 m by geophysical studies (Hustoft et al., 2009; Knies et al., 2004; Rajan et al., 2012; Westbrook et al., 2009). This area is strongly affected by the northward-flowing West Spitsbergen current (Walczowski et al., 2005) which warmed by 1 °C over the last 30 years (Schauer et al., 2004). According to Westbrook et al. (2009), the observed gas release might be a response to this recent warming and might have caused emission of about 0.027 Tg CH_4 yr^{-1}. However, it is questionable if the CH_4 reaches the atmosphere because of gas bubble dissolution and microbial oxidation in the water column. To answer this question, we conducted a study in an active gas ebullition area offshore Spitsbergen to investigate the potential pathways of gas seepage released methane. The mass transfer of CH_4 from rising gas bubbles into the ambient water column was calculated by a gas dissolution model (McGinnis et al., 2006, 2011) and the subsequent transport and microbial oxidation of the dissolved CH_4 were investigated by comparing hydroacoustic data with oceanographic and geochemical data.

2. Regional settings

2.1. Geology and seepage

The study area is located on the continental slope 22.5 km west of Prins Karls Forland (Spitsbergen) between Kongsfjorden and Isfjorden (Fig. 1). Previous investigations detected a prominent moraine system formed by glacial erosion or glaciotectonic detachment of larger blocks or sediments (Landvik et al., 2005). The investigated area with a mean water depth of 245 m is located close to the shelf edge with a steep slope located to the east and a less steep slope located to the north of the study area (Fig. 1). The gas hydrate stability zone tapers out at a sediment depth of about 400 m (Westbrook et al., 2009). The presence of shallow gas accumulations and pockmarks in this area was suggested by Rajan et al. (2012) who applied high-resolution mapping of the seafloor. The study area is the northernmost section of the region investigated by Rajan et al. (2012) and Westbrook et al. (2009),

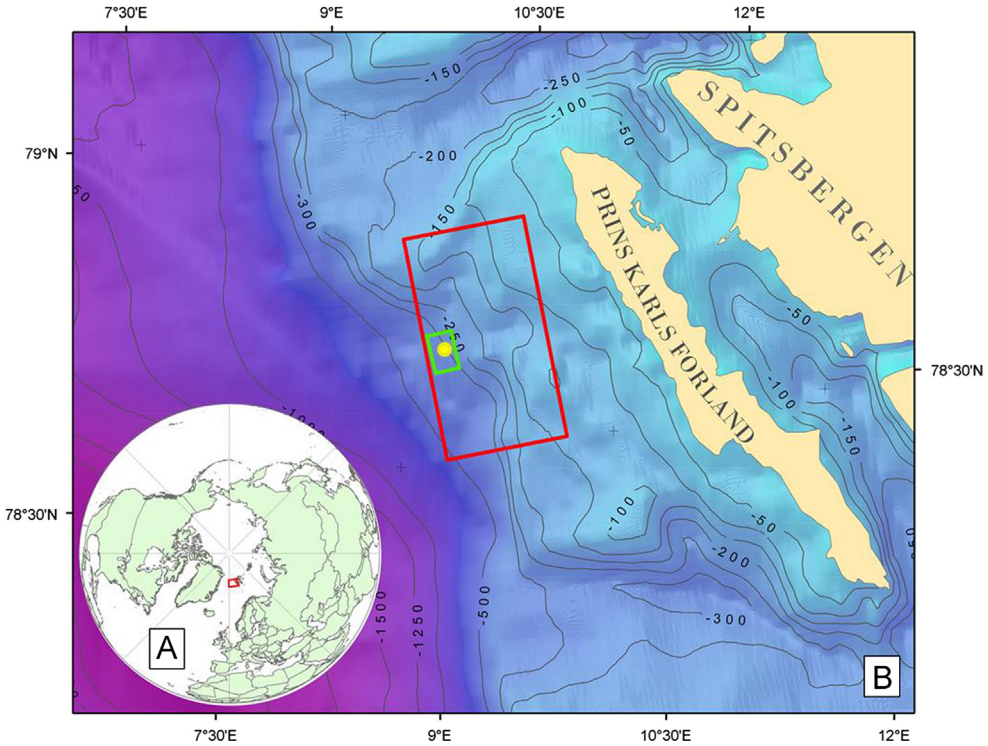

Fig. 1. (A) Global view of the study area west of Spitsbergen. (B) The area investigated by Westbrook et al. (2009) is shown as red rectangle, the detailed study area (green rectangle) and the crossing point of the CTD-transects (yellow dot). Bathymetry is taken from the International Bathymetric Chart of the Arctic Ocean (IBCAO). The contour lines show the water depth and the light blue coloured area indicates the shelf bank.

who both observed gas ebullition into the water column by hydroacoustic. The highest methane concentration of 42 nmol L^{-1} was reported for a gas flare close to the seabed (~230 m water depth) according to Westbrook et al. (2009). In contrast to the high methane concentrations close to the seafloor the observed background concentration of dissolved CH_4 in the mid and surface water is about 10 nmol L^{-1}. This is significantly exceeding the background values of most parts of the ocean, e.g. a background of 2.5–3.5 nmol L^{-1} was reported for Atlantic Ocean water (Rehder et al., 1999) and points to methane release from several intergranular seepages or micro-seepages sites widely spread over the continental shelf (Damm et al., 2005).

2.2. Hydrography

The oceanographic conditions in the study area are controlled by the West Spitsbergen Current (WSC), which transports Atlantic Water (AW) northwards along the shelf edge (Schauer et al., 2004). The Coastal Current (CC) as an extension of the East Spitsbergen Current might introduce less saline water than the Atlantic Water into the study area (Saloranta and Svendsen, 2001). In addition, seasonal events like formation and melting of sea ice or glaciers, river run off from Spitsbergen, fjord outflow, and special events like storm activities influence the hydrography of the study area causing strong seasonal variations. The WSC is stratified throughout the summer, but vigorous convection vertically mixes the AW within the WSC during winter (Cisewski et al., 2003).

3. Sampling and analytical procedures

During the expedition HE 333 in August 2010, the water column was investigated by hydroacoustic surveys, geochemical analysis of water samples, and by oceanographic data recording. In total, 175 km^2 (Fig. 1) were surveyed with a split beam fish finder sonar (EK 60 by Simrad) to detect gas flares. In addition, 145 discrete water samples were collected using a CTD/Rosette sampler system at 22 stations and shallow-towed (10 m water depth) high-resolution mapping of CH_4 was carried out with an underwater mass spectrometer (UWMS).

3.1. CTD casts and water sampling

In total 13 vertical CTD-casts were conducted to collect water samples and oceanographic data by a system consisting of a Rosette sampler equipped with 12 10-L-Niskin bottles, a Seabird SBE 911 conductivity/temperature/depth (CTD) profiler, a Seabird SBE 43 oxygen (O_2) sensor, and a Benthos PSA-916 altimeter. A south–north (S–N) transect and an east–west (E–W) transect were sampled crossing at a point, where most gas flares were observed (Fig. 1). Additionally, 9 CTD casts were obtained by towing the instrumentation at 2 m, 10 m, and 20 m (±1 m) above the seafloor to acquire more water samples and oceanographic data at greater depths. The system was adjusted via the altimeter to a defined distance from the seafloor. To flush the Rosette water sampler, the device was heaved and lowered before each sampling.

3.2. Water measurements

3.2.1. Dissolved CH_4 concentration

A novel underwater membrane inlet mass spectrometer (UWMS) was applied for on-board measurements of dissolved gases as well as high resolution mapping of CH_4 concentrations at 10 m water depth (Gentz and Schlüter, 2012). The UWMS allows high sampling frequency (every 2 s) and therefore has high spatial resolution to detect variability in methane concentrations. Furthermore, standard gas extraction by gas chromatography and analysis were performed on board.

Water samples were immediately taken from the Niskin bottles and analyzed by the UWMS to obtain simultaneous measurement of dissolved CH_4, nitrogen (N_2), O_2, and argon (Ar). The mass spectrometer (Bell et al., 2007; Short et al., 2001, 1999) consists of a membrane inlet system, a quadropole mass analyzer, a turbo pump and a newly designed cryotrap (Gentz and Schlüter, 2012) which lowers the detection limit of CH_4 from more than 100 nmol L^{-1} to 16 nmol L^{-1} (Schlüter and Gentz, 2008). During the operation of the UWMS, water is continuously pumped (3 ml min^{-1}) via a peristaltic pump (KC Denmark) to the heated (50 °C) membrane inlet system (MIS), where gas permeation takes place. The benefit of this instrument is that the samples can be measured directly without any sample preparation within less than 2 min. Due to the fast data availability of the dissolved methane concentrations, cruise and mission planning could be optimized on board in a short time.

Discrete water samples collected by the Rosette water sampler were analyzed for CH_4 concentrations, $\delta^{13}C_{CH_4}$ values, and microbial CH_4 oxidation rates. CH_4 concentrations were analyzed by mass spectrometer and gas chromatography (Kampbell et al., 1989). For gas chromatography measurements, the water samples were taken immediately from the Niskin bottles and transferred into 20 ml glass vials, capped with a Teflon septum, and crimped gas tight. A head space of 5 ml volume was introduced by injecting Ar gas. After 5 h of equilibration, the gas concentration in the head space was analyzed by using the gas chromatograph TraceGC (Thermo Finnigan; Waltham, USA), equipped with a flame-ionization detector and a Porapak Q column. The GC oven was operated isothermally at 100 °C and the temperature at the sample inlet was 300 °C. Two standard gases (10 ppm and 1000 ppm) were used for the calibration. Based on the CH_4 concentration in the head space and the CH_4 concentration in the aqueous phase, which was calculated using the Bunsen coefficient (Wiesenburg and Guinasso, 1979), the CH_4 concentration in the water sample was derived. The overall error of the method was about 5%.

A detailed cross validation of the methane concentrations derived by the GC and UWMS was done by Schlüter and Gentz (2008). The results reveal a close correlation of both analyzing techniques; something which was verified in this study.

3.2.2. Stable carbon isotopic ratio

For measurements of the carbon isotopic ratio of CH_4, the water samples were taken immediately from the Niskin bottles. The dissolved gas was extracted from the water samples by vacuum-ultrasonic treatment (Schmitt et al., 1991). This method achieved 63% recovery of the total dissolved CH_4 (Lammers and Suess, 1994). The $\delta^{13}C_{CH_4}$ values were determined by a Delta XP plus Finnigan mass spectrometer. The extracted gas was purged and trapped with PreCon equipment (Finnigan) to pre-concentrate the sample. All isotopic ratios were given in a δ-notation relative to the Vienna Pee Dee Belemnite (VPDB) standard (Craig, 1957). Depending on the CH_4 concentration, the reproducibility derived from duplicates was 0.5–1‰ VPDB.

3.2.3. CH_4 oxidation rate

At the station where the S–N and E–W transects cross (CTD 34, 78°39.14 N and 9°25.93 E, yellow dot in Fig. 1) additional water samples were taken for CH_4 oxidation rate measurements throughout the water column. All samples were collected in 100 ml crimp-top sample bottles, which were flushed with two volumes of water and filled completely to exclude bubbles. At each chosen water depth, two samples were taken and at every other water depth, an additional control sample was collected. Control

samples were treated by injecting saturated mercury chloride ($HgCl_2$) to stop metabolic processes before tracer injection. 50 μL of [^{3}H]–CH_4 (ARC Inc., 0.37–0.74 TBq mmol^{-1}) was injected in each sample as described in Valentine et al. (2001) raising the ambient CH_4 concentrations by 1–2 nmol L^{-1}. The samples were subsequently shaken for ~10 min on an orbital shaker and incubated in the dark at 2 °C. Incubations were stopped after 3 days, a 1 mL aliquot of each sample was taken and mixed with 5 ml Ultima Gold scintillation cocktail for analysis in a liquid scintillation counter (Single Sample LSC, Betascout Hidex) on board to determine the total radioactivity injected. Then, the sample was sparged for ≥30 min with N_2 gas to remove remaining [^{3}H]–CH_4. Samples were capped again and stored at 4 °C until further analysis. The residual radioactivity of [^{3}H]–H_2O was measured in the laboratory (Packard Tri-Carb LSC). All measurements were corrected for quench effects and for differences associated with the different counters used. From the corrected value, the amount of ^{3}H that remained in the water in control experiments (0.2 ± 0.1%) was subtracted. Ninety per cent of biological replicate samples differed by < 30%. CH_4 oxidation rates (r_{OX}) were calculated assuming first order kinetics as described in Valentine et al. (2001).

$$r_{OX} = k'[CH_4] \quad (1)$$

where k' is the effective first order rate constant calculated as the fraction of labelled CH_4 oxidized per unit time and [CH_4] is the ambient CH_4 concentration.

3.3. Hydroacoustic data acquisition

A fish finder sonar system (Simrad EK60) operated at 38 kHz was used to detect and map the horizontal and vertical distribution of gas flares in the water column. For unambiguous identifications of gas vents the protocol suggested in Judd et al. (1997) with following criteria were applied: The gas flares have to touch the seafloor, which is considered to be the origin of gas ebullition; to exclude fish schools, the vertical to horizontal dimension ratio of the echo pattern must be greater than two; and isolated flares are only included if detected at least twice at the same location.

3.4. Bubble gas exchange modelling

The gas bubble dissolution model by McGinnis et al. (2006, 2011) optimized by Dan Frank McGinnis for the regional settings was applied to estimate the maximum height of ascending bubbles and the transfer of released methane from gas bubbles into the water column. Model simulations were compared to the acoustic images of gas flares and the discrete dissolved CH_4 concentrations of water samples collected using CTD-casts.

4. Results

4.1. Flare imaging

The flare imaging was conducted to locate active gas bubble ebullition sites in the study area, thus, supporting the geochemical sampling of CH_4 anomalies in the water column in close vicinity to the seeps.

At least 4 transects show acoustic evidence for gas release in the study area (Fig. 2). In S–N direction, 10 gas flares were observed in water depths of 242–258 m along a distance of 11.5 km (Fig. 2A, Table 1). All three transects in E–W direction (Fig. 2B,C,D) confirm that most of the gas flares are lined up in S–N direction and accompanied by some mid-water biological scatter. The flare backscatter intensities peak around 50 m rise height and decay above. The minimum measured rise height is also 50 m and the maximum detectable rise height was up to 200 m (Fig. 2A). These observations of the gas flare locations as well as the maximum rise heights match with the observations by Westbrook et al. (2009). Even though the majority of the flares presented in Fig. 2 only rise until 150 m water depth, the bulk bubble rise height might be even higher considering beam geometry and sampling bias suggested in Schneider von Deimling et al. (2011).

From the tilt of the plume in the S–N transect together with an estimated bulk bubble rise velocity of 0.08–0.25 m s^{-1} we estimated a water velocity of 0.3–0.5 m s^{-1} in northerly direction resulting in a short residence time of the bottom water at the S–N transect between 0.27 and 0.44 d.

4.2. Water masses in the study area

The CTD data of 13 vertical profiles and 9 horizontal transects collected on two consecutive days in August 2010 illustrate the oceanographic conditions in the study area during the survey (Fig. 3). The water mass classification described by Slubowska-Wodengen et al. (2007) was applied to identify three distinct layers. A surface layer (0–40 m) herein later on referred to as Layer I consisted of fresh Polar Water (PW, Salinity (S) < 34.4). Layer II below (40–225 m) displays a mixture of subsurface, dense shelf water (ASW, $34.4 \le S \le 34.9$), Lower Arctic Intermediate Water (LAIW, $S > 34.1$, $T > 3$ °C), and shallow Atlantic Water (AWs, $S > 34.90$, $T > 3.6$ °C).

Layer III (AWd, $S > 34.90$, $T < 3.6$ °C) comprises the water from the seafloor to 20 m above the seafloor (Figs. 4 and 5). This layer is characterized by a maximum salinity of 35.02, an internal potential density of 27.885 kg m^{-3}, a minimum temperature of 3.16 °C, and O_2 concentration of up to 6.60 ml L^{-1} (Figs. 4 and 5).

4.3. CH_4 concentrations, microbial CH_4 oxidation rates, and stable carbon isotopic ratios

4.3.1. Vertical sampling of the water column

Water samples for CH_4 concentrations, $\delta^{13}C$ values, and CH_4 oxidation rate measurements were collected at station 34 (78°39.14 N and 9°25.93 E, Fig. 6) situated at the same location, where Westbrook et al. (2009) previously sampled water within a gas flare for methane analysis. The CH_4 concentration decreases from 48 nmol L^{-1} close to the seafloor to local background concentration of ~10 nmol L^{-1} (Damm et al. 2005) at 175 m water depth. Then it remains at this concentration level throughout the water column. This methane concentration profile is similar to the observations by Westbrook et al. (2009). The methane in Layer III, compared to the methane in Layer I and II, is depleted in ^{13}C (Fig. 6A), nevertheless the variation is in larger range (Fig. 6A). Microbial CH_4 oxidation was enhanced in Layer III compared to the other layers above (Fig. 6B). CH_4 oxidation rates of 0.77 ± 0.2 nmol L^{-1} d^{-1} corresponding to elevated CH_4 concentrations of 42.3 ± 2 nmol L^{-1} (Fig. 6A) were measured in Layer III. In Layer I and Layer II, CH_4 oxidation rates were < 0.22 nmol L^{-1} d^{-1} corresponding to CH_4 concentrations of < 25.2 nmol L^{-1}. This results in a much faster turnover time of the methane in the deep Layer III if compared to much longer turnover times in Layer II and Layer I (Fig. 6B).

Above the gas flares in a water depth of 10 m (green box in Fig. 1), the UWMS was deployed to measure dissolved CH_4 concentrations with high spatial resolution. These continuous measurements support the observations that CH_4 concentrations remain below the detection limit of 16 nmol L^{-1}. This supports that no significant additional methane is observed near the sea surface that

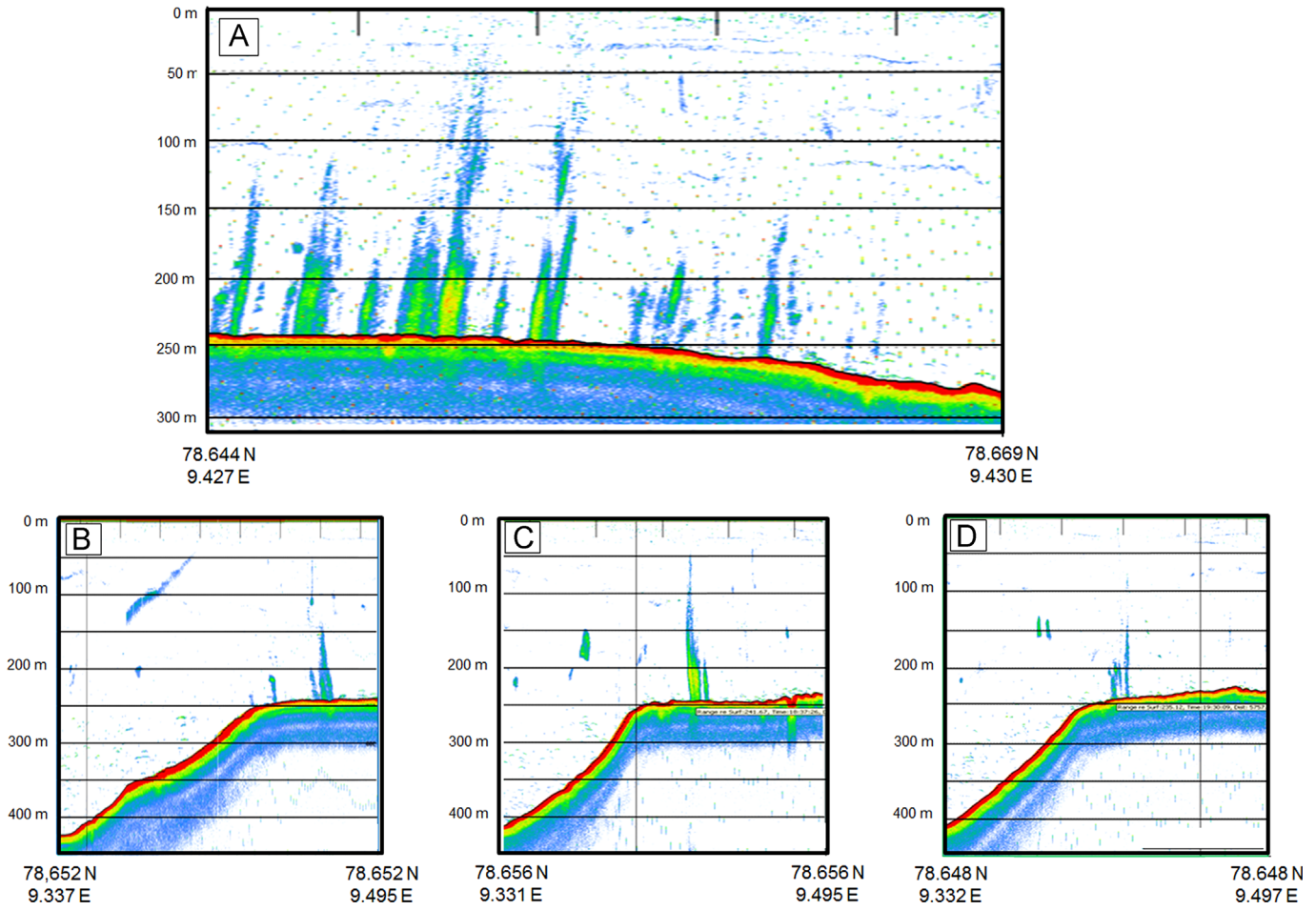

Fig. 2. (A) Flare images (EK 60, Simrad) of the gas flare transect 1 in S–N and transects in E–W direction (B, C and D).

Table 1
Location and water depth of the observed flares with an estimated error of ±0.003 N and ±0.01 E.

Depth [m]	Latitude [DD]	Longitude [DD]
258	78.661 N	9.437 E
248	78.657 N	9.434 E
246	78.654 N	9.432 E
243	78.654 N	9.433 E
242	78.653 N	9.433 E
242	78.651 N	9.432 E
243	78.650 N	9.431 E
242	78.649 N	9.431 E
242	78.647 N	9.432 E
249	78.645 N	9.432 E

could have been transported through e.g. local bubble-mediated upwelling with enhanced bubble lifetime (Solomon et al., 2009).

4.4. Detailed sampling of the dissolved CH_4 concentrations in the bottom water (Layer III) and stable carbon isotopic ratios

Besides the vertical distribution of CH_4 in the water column, a spatially high resolution survey of dissolved CH_4 concentrations in 2 m, 10 m, 20 m above the seafloor was conducted crossing the gas flares shown in Figs. 2 and 7A. The CH_4 concentrations range between 15 and 524 nmol L^{-1} (Fig. 7). Highest concentrations of 346 and 524 nmol L^{-1} were observed 2 m above the seafloor (green and blue dot in Fig. 7B); the average CH_4 concentration at this depth is 70 nmol L^{-1}, which is the highest average in the entire water column. 10 m above the seafloor, the highest CH_4 concentration is 140 nmol L^{-1} while the average concentration decreased to 40 nmol L^{-1}. The CH_4 concentrations at 20 m above the seafloor are less than 30 nmol L^{-1} except of one sample with 50 nmol L^{-1}. The average concentration is 12 nmol L^{-1}, which is close to the background concentration of CH_4 in the study area (Fig. 7D).

The $\delta^{13}C_{CH_4}$ values of all samples of the entire water column range between −37.5‰ and −61.6‰ VPDB (Fig. 8A, B). These results were compared to the measured inverse CH_4 concentration of the same samples (Fig. 8A). This Keeling plot point out that increasing depletion in $\delta^{13}C$ is related to increasing CH_4 concentration (Fig. 8A). Additionally, the $\delta^{13}C_{CH_4}$ values in Layer II and Layer I range just in between −39.71‰ and −43.55‰ VPDB (red dots in Fig. 8A), while the $\delta^{13}C_{CH_4}$ values in Layer III varies in a wider range of −37.5‰ and −61.6‰ VPDB (black dots in Fig. 8A). According to Faure (1986) the slopes of the linear regression curves (Fig. 8A) indicate that the CH_4 in Layer III is a mixture of two end members, while in Layer II and Layer I only one source could be identified.

In Layer III ^{13}C depleted C–CH_4 was found mainly along the S–N transect with $\delta^{13}C_{CH_4}$ values from −61.6‰ to −52.6‰ VPDB (mean −59.5‰ VPDB). In contrast, more ^{13}C enriched C–CH_4 was found along the E–W transect where the $\delta^{13}C_{CH_4}$ values range between −37.5‰ and −52.9‰ VPDB (mean −42.4‰ VPDB; Fig. 8B).

In the S–N direction, sampling was performed in line with the gas flares and water current direction. This is evident by CH_4 concentrations increasing from 48 to 346 nmol L^{-1}. In the E–W

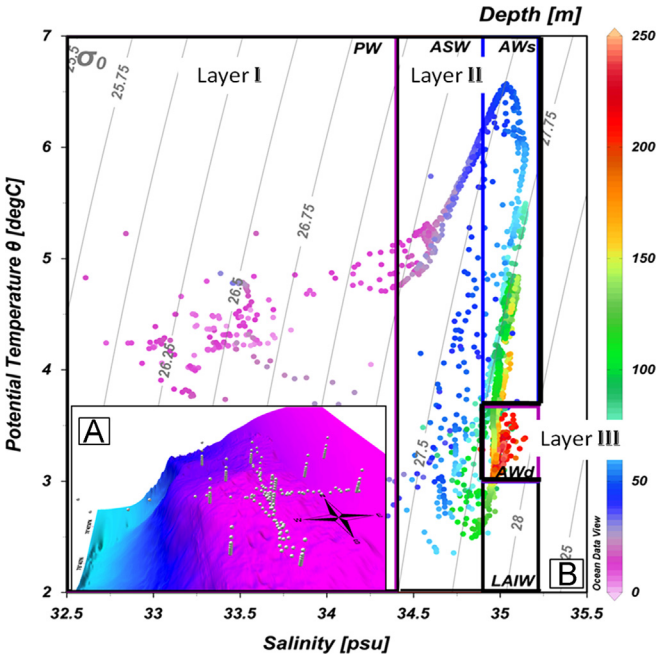

Fig. 3. (A) 3D view of the bathymetry showing vertical and horizontal CTD sampling positions at the shelf bank close to the shelf edge. (B) Potential temperature versus salinity (*T*/*S*) plot based on all CTD measurements collected in the study area for identification of water masses according to the classification of the water masses by Slubowska-Wodengen et al. (2007). The colour of the dots indicates the water depths. Layer I (surface layer) consists of Polar water (PW). Layer II is a mixture of Arctic surface water (ASW), surface Atlantic Water (AWs), and lower Arctic Intermediate Water (LAIW). Layer III, the lowermost water mass, consists of deep Atlantic water (AWd). Graphic created by Ocean Data View (R. Schlitzer, Ocean Data View, 2011, http://odv.awi.de).

direction, the CH_4 concentrations of 16.4 and 39.4 nmol L^{-1} and the $\delta^{13}C_{CH_4}$ near background values show less influence of the dissolved methane distribution at the gas flares if compared to the S–N direction. In addition to spatial variations, both CH_4 concentration and $\delta^{13}C_{CH_4}$ show temporal fluctuations. At the intersection of both transects, sampling was carried out in Layer III three times within 24 h (red circle in Fig. 8B). Values shift from −38‰ VPDB and 139 nmol L^{-1} at the first measurement (21.08.2010; 18:00) to −57‰ VPDB and 109 nmol L^{-1} at the second measurement (22.08.2010; 12:32) to −53‰ VPDB and 64 nmol L^{-1} (22.08.2010; 14:13) at the third measurement.

5. Discussion

5.1. Gas ebullition as a source for dissolved CH_4 in the water column

In the study area we consider the release and the rise of methane loaded gas bubbles from the seafloor as the main source for dissolved CH_4 in the water column. Initially, CH_4 loaded gas bubbles are supersaturated compared to the ambient water composition, and consequently CH_4 is transported out of the bubble (dissolution) until the dynamical equilibrium is reached. Simultaneously, major gases like N_2, O_2 or CO_2 dissolved in the seawater are supersaturated with respect to the initial composition of the gas bubble, which causes a mass transfer of these gases into the gas bubble (stripping). These processes were modelled by e.g., Leifer and Judd (2002), Leifer and Patro (2002) and McGinnis et al. (2006, 2011) to estimate the mass transfer kinetics between a single gas bubble and seawater, i.e. fractional changes of the respective gases during the ascent of a CH_4 gas bubble from the seabed towards the sea surface.

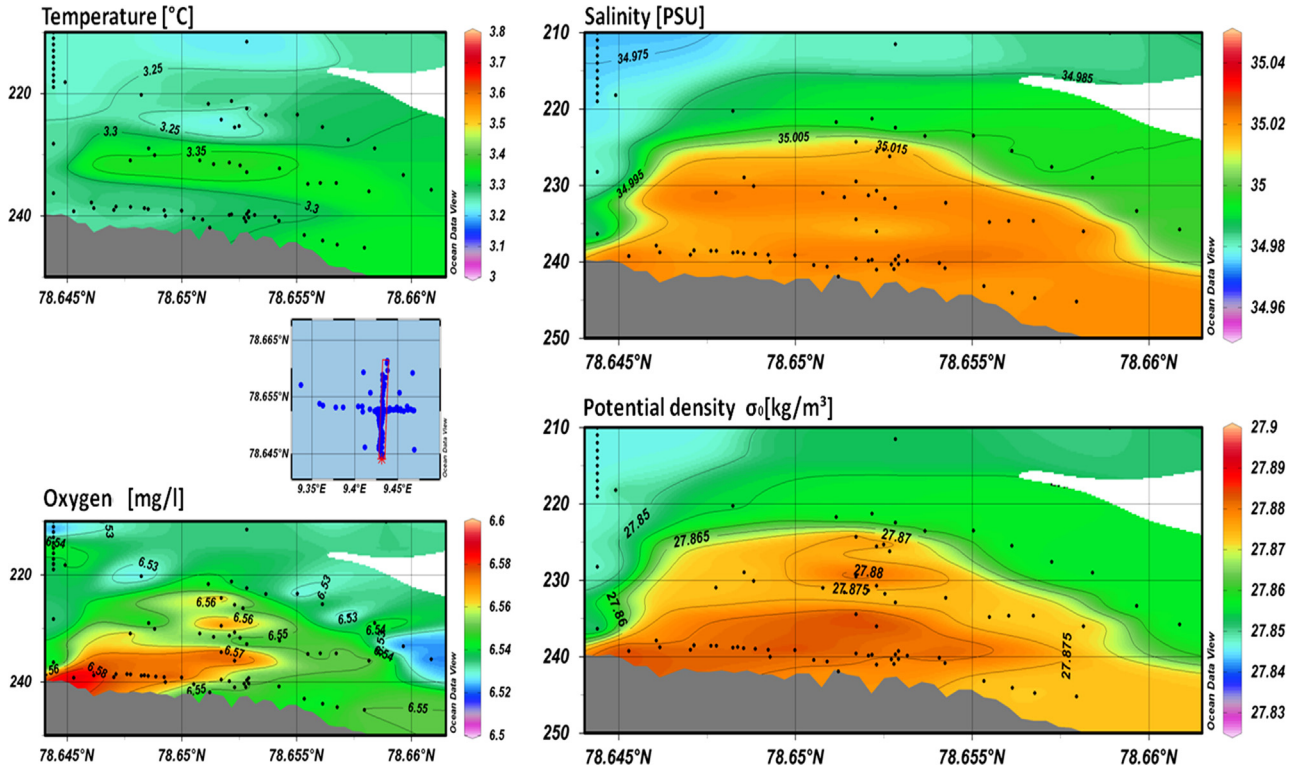

Fig. 4. Oxygen concentrations, salinity, temperature, and the potential density indicate the extent of Layer III, i.e., deeper Atlantic water (AWd), in S–N direction. Graphic created by ODV.

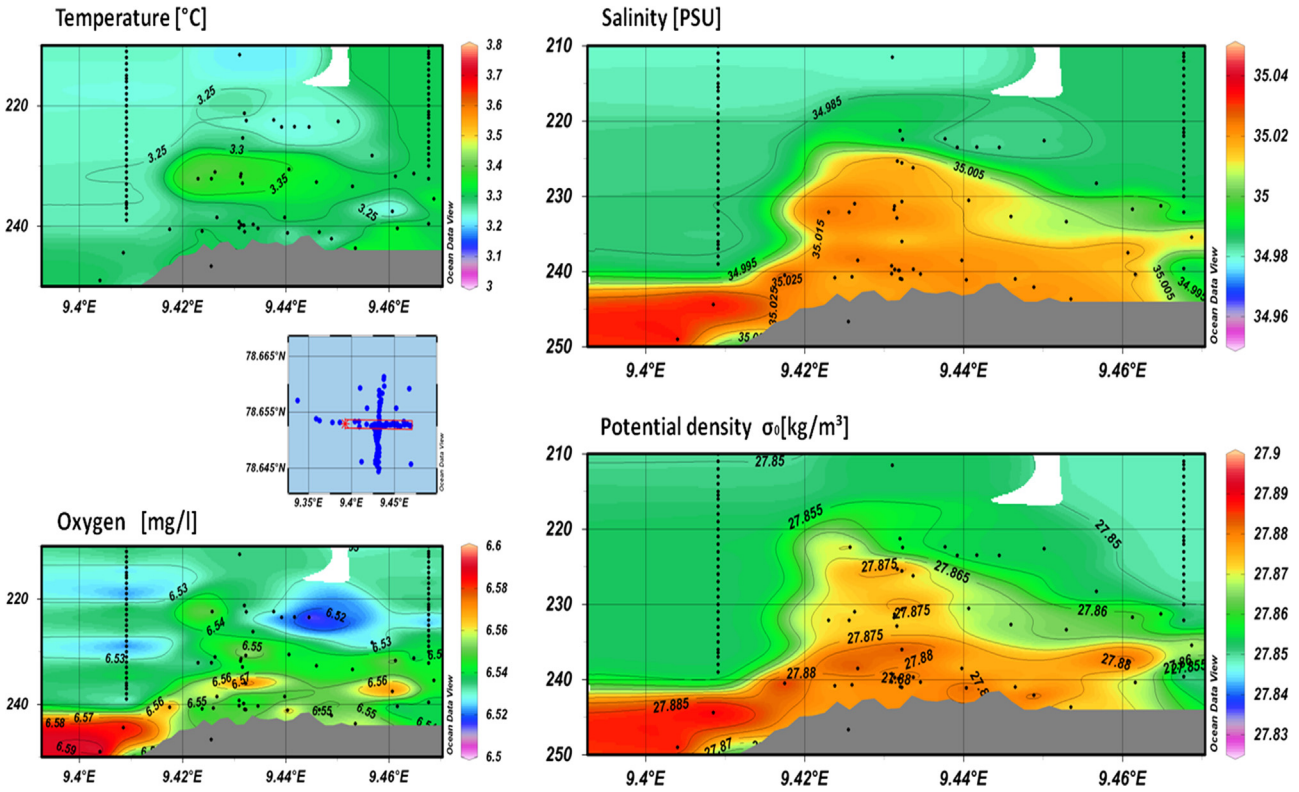

Fig. 5. Oxygen concentrations, salinity, temperature, and the potential density indicate the extent of Layer III, i.e., deeper Atlantic water, in E–W direction. Graphic created by ODV.

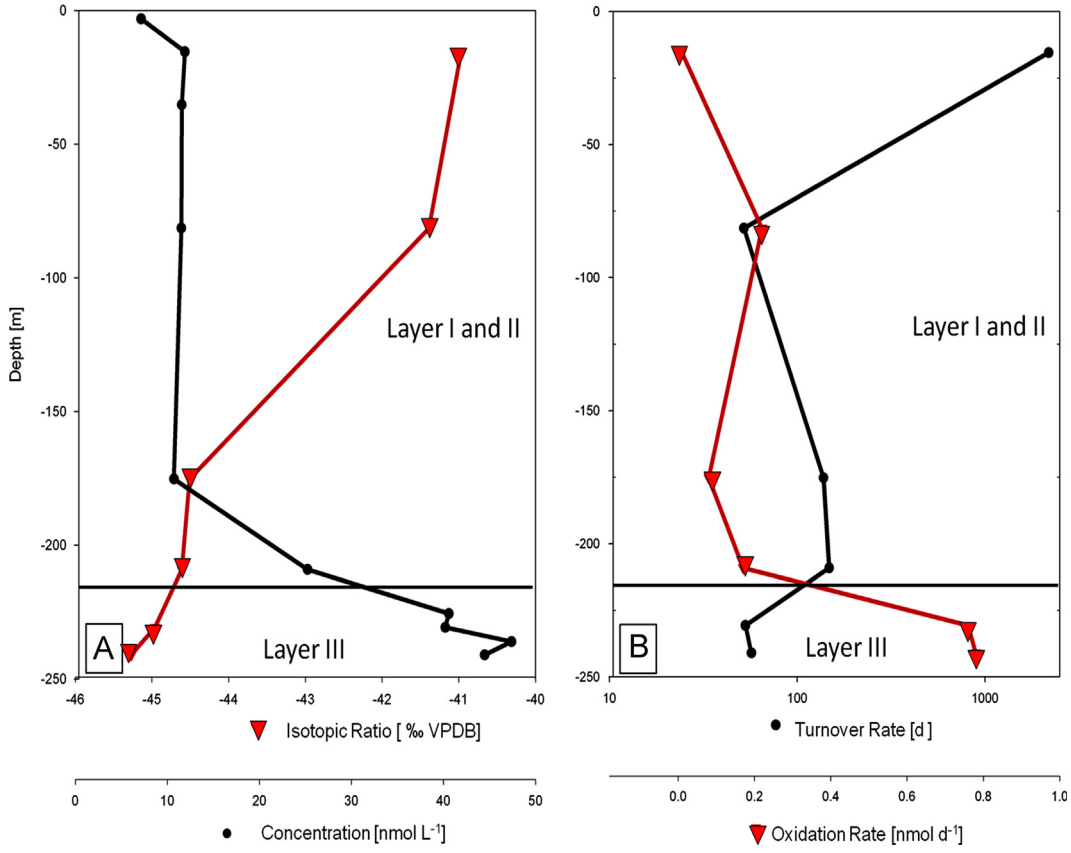

Fig. 6. Profiles of station 34 (A) CH_4 concentration (black dots) and isotopic ratio (red triangles). (B) Microbial CH_4 oxidation rates (red triangles) and turnover times (black dots).

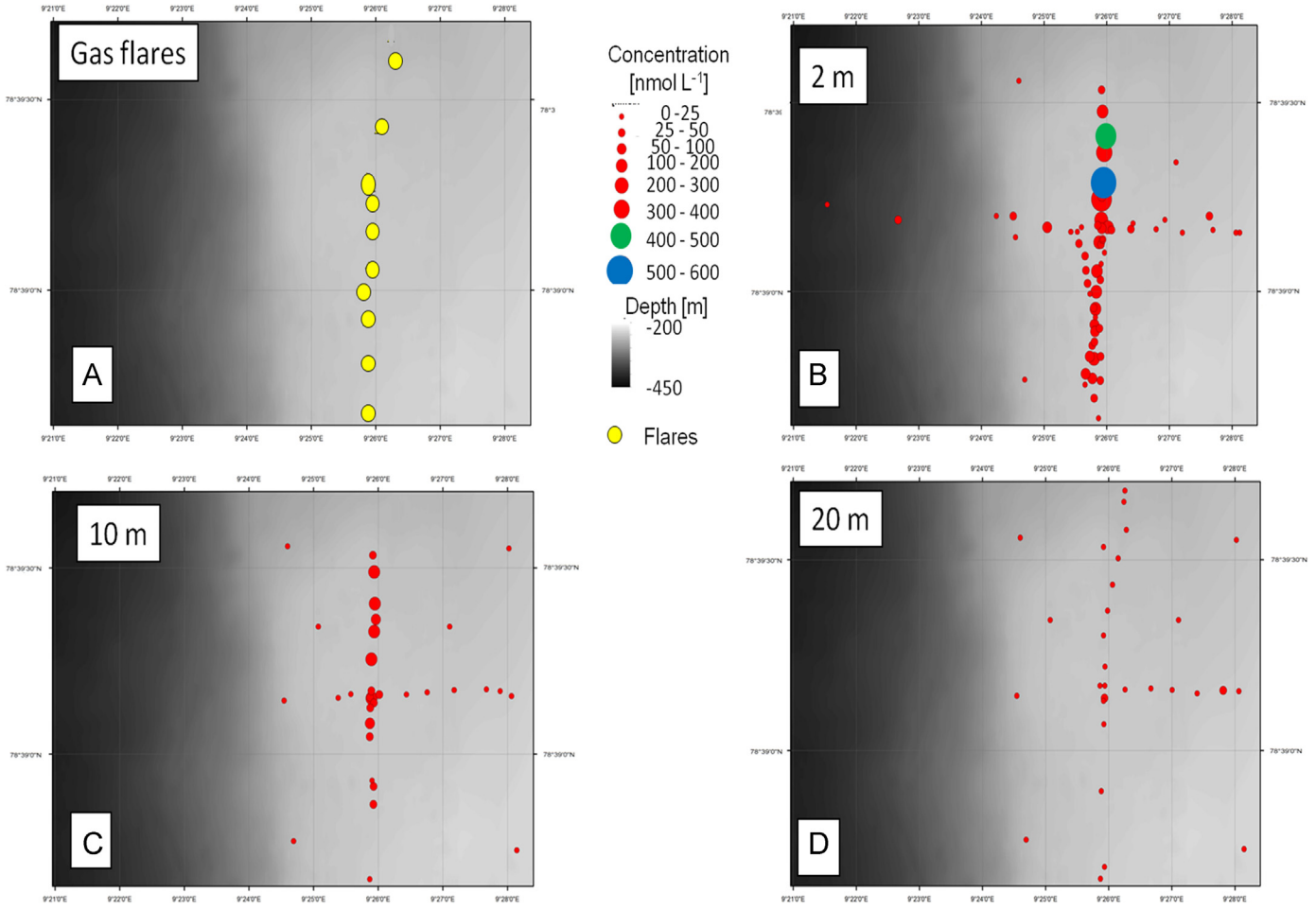

Fig. 7. Positions of the observed gas flares (A) and CH_4 concentrations in 2 m (B), 10 m (C) and 20 m (D) above the seafloor.

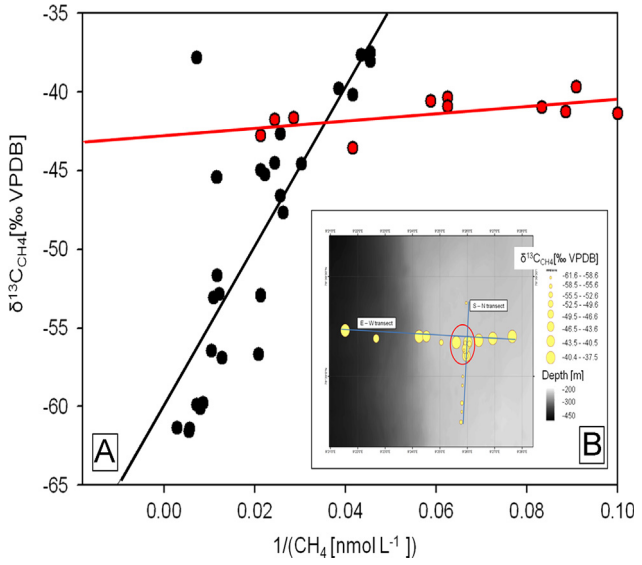

Fig. 8. (A) Inverse CH_4 concentration versus $\delta^{13}C_{CH_4}$ values (Keeling plot). Layer III is presented by black dots and Layer II and Layer I by red dots. (B) Distribution of $\delta^{13}C_{CH_4}$ 2 m above the seafloor including the transect lines. The red circle indicates the crossing zone of the two transects.

As an example, we considered the relation between the dissolution of the gas bubbles and the change in gas composition during the bubble rise derived by the use of a model based on the results of McGinnis et al. (2006, 2011) with the highest gas bubble rise heights observed by hydroacoustic (Fig. 9B). Input parameters of the model were initial bubble size, initial CH_4 fraction in the gas bubble as well as salinity, temperature, O_2, and CH_4 concentrations in the water column. The parameters were derived from CTD cast 34 which was obtained next to a gas flare in the study area and we assumed that the initial gas bubbles consist of CH_4 only.

The calculated initial bubble diameter to reach the water surface would have to be larger than 11.05 mm. Considering the maximum acoustically derived rise height of 200 m in the water column (Fig. 9B) an initial bubble diameter of at least 10.25 mm (Fig. 9A) would be required. For this case, 99.99% of the methane in the gas bubble would be dissolved below 150 m. This suggests that no CH_4 could be transferred directly into the atmosphere via bubble transport in the study area. In the study area, a 5 mm bubble would rise up 69.5 m (Fig. 9A) which is comparable to the observed flare backscatter intensities of the gas flares. The dissolution of the CH_4 takes place so quickly that, after rise of 20 m, only ~20% of the initial CH_4 is left in the bubble (Fig. 9A).

Given the vertical dissolved CH_4 concentrations-distribution and the pronounced pycnocline (Fig. 10) we suggest that the elevated methane concentrations in the Layer III mainly derives from dissolving methane gas bubbles during the first 20 m rise height. The distinct methane concentration gradient points to smaller gas bubbles than 5 mm (Fig. 9B), but could also be explained by lower current speed and longer methane accumulation time during the travel of bubbles through Layer III. Therefore, we assume that ~80% of the seabed released CH_4 via gas bubble is dissolved below the pycnocline in Layer III. Nevertheless, the

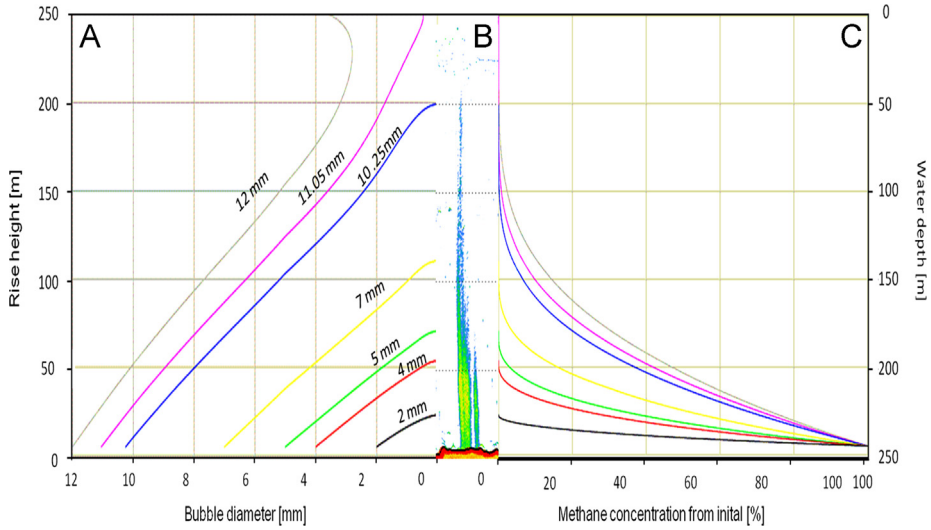

Fig. 9. Decrease of the bubble diameter during the ascent from the seafloor for initial bubbles sizes of 2–12 mm (A) compared with the hydroacoustic image of the highest detected gas flare (B). Decrease of the initial CH_4 concentration in the bubbles during their rise in the water column (C).

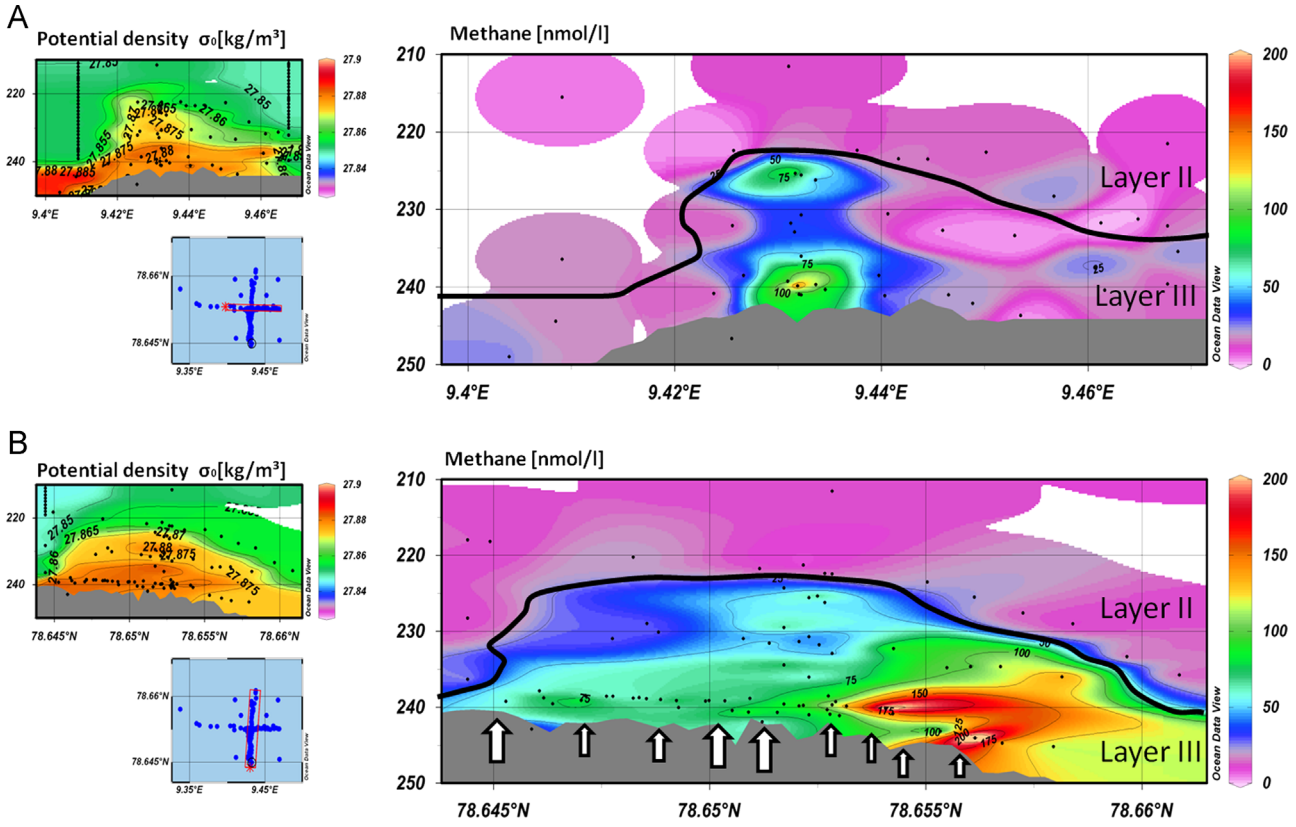

Fig. 10. Dissolved CH_4 in the lower water column indicates the dominance of lateral transport. The pycnocline is indicated though black lines. (A) E–W transect, the plumes spreads inside Layer III in flow direction. A strong concentration gradient is seen between Layer III and II. (B) S–N transect – vertical spreading of the plume appears restricted. White arrows in (B) indicate the position of the observed gas flares.

impact of dissolved fluid flow and/or diffusive methane source strength remains to be investigated.

5.2. *Pathways and origin of CH_4 in the water column*

Flare imaging and model results indicate that almost no CH_4 reaches the atmosphere via the transport of gas bubbles. Hence, the majority of the CH_4 is dissolved in the ambient water. In the bottom water, CH_4 concentrations decrease by 93% within 6 m vertical distance, from 142 nmol L^{-1} at 15 m above the seafloor to 10 nmol L^{-1} at 21 m above the seafloor (Fig. 10). Such a large decrease in CH_4 concentration cannot be explained by bubble dissolution only (see model results above). Already 21 m above the seafloor the CH_4 concentrations are as low as the local background concentration hinting to a restricted vertical transport.

Pycnoclines strongly hamper vertical eddy diffusive transport and mixing thus fostering lateral transport in the same density layer (Damm et al., 2005; Schmale et al., 2010; Schneider von

Deimling et al., 2011). In the study area, a salinity gradient generates a density gradient at ~20 m above the seafloor. As a consequence CH_4 is dispersed dominantly in Layer III. Therefore, exclusively in Layer III CH_4 concentrations higher than 50 nmol L^{-1} were detected. AWd, the water mass that defines Layer III, extends from the seafloor up to 20 m above the seafloor and was found along the transects in E–W and S–N direction (Figs. 3 and 10). This water mass is part of the West Spitsbergen current (WSC) which flows northward east of the shelf edge and we assume that a part of this water mass is intruded onto the shelf bank by eddy overturning (Tverberg and Nost, 2009).

According to the flow directions of the WSC (Piechura et al., 2001; Walczowski et al., 2005) and the ESC (Saloranta and Svendsen, 2001), the CH_4 enriched Layer III flows northward on the shelf bank alongside the shelf edge. In the S–N direction, the vertical restriction of Layer III is confirmed by oceanographic changes (Fig. 4): increase in temperature (~0.13 °C) and a decrease in salinity (S~0.1).

In addition, the extent of the CH_4 plume in northern direction matches with the current direction. The CH_4 plume (concentrations > 25 nmol L^{-1}) is restricted in the E–W direction to the area where gas release is observed (Fig. 10B). The E–W extent of the plume is much smaller than the E–W extent of Layer III (Fig. 2). These results indicate that mixing in the E–W direction is limited due to the rapid transport by the WSC to the north direction.

The assumption of the rapid transport is supported by $\delta^{13}C_{CH_4}$ measurements, which are commonly used to describe the potential fate of CH_4 due to mixing with background CH_4 or microbial oxidation of CH_4 in the water column. We assume that the variations in isotopic composition (up to 19‰ VPDB over a small area) in the water column do not reflect any isotopic fractionation which occurs in the water column when CH_4 is oxidized (Fig. 6A), which is most likely due to the short residence time of the water above the seafloor (max. 0.44 d). This is supported by the interpretation of the Keeling plot (Fig. 8), we suggest that the isotopic heterogeneous CH_4 by time and region is related to mixing. The regression line in the Keeling Plot (Fig. 8) points to a mixing of CH_4 released from the gas bubbles with $\delta^{13}C_{CH_4}$ values of around −60‰ VPDB and background CH_4 of the inflowing water mass with $\delta^{13}C_{CH_4}$ values of around −40‰ VPDB (Faure, 1986). Nevertheless, a mixture of different gas types i.e. thermogenic and biogenic source types are likely (Knies et al., 2004), however, the isotopic signature of CH_4 detected in the water column cannot contribute to resolve this question.

Although microbial oxidation does occur, the oxidation rate in Layer III (0.78 ± 0.22 nmol L^{-1} d^{-1}) is 3 times higher compared to Layer II (< 0.22 nmol L^{-1} d^{-1}) only a small fraction of the CH_4 is oxidized in the study area. If we consider the average concentration of 48.8 nmol L^{-1} in Layer III and a residence time of the water mass below 0.44 d, 99.3% of the CH_4 will be laterally transported out of the study area. If the advective transport is neglected, all methane in the surveyed box defined by the S–N and E–W transects would be microbially oxidized in 50–100 d. This is comparable to microbial oxidation in the Coal Oil Point plume (Mau et al., 2012) and the rapid consumption of the methane after the Gulf of Mexico oil spill (Kessler et al., 2011).

However, due to restricted vertical transport and the short residence time of the water mass of Layer III above the gas ebullition area, most of the stripped CH_4 is rapidly transported northward away from the study site within the bottom water and presumably microbially oxidized along its path. Nevertheless, the local CH_4 background concentration of ~10 nmol L^{-1} in Layer II (Damm et al., 2005; Westbrook et al., 2009) is considerably enriched compared to the ocean background concentration (Rehder et al., 1999). We assume that the CH_4 in Layer II is a mixture of CH_4 originating from dissolution of rising gas bubbles and surface water enriched in CH_4 from several other sources like inter-granular seepages or micro-seepages occurring widely spread over the shelf (Damm et al., 2005). This assumption is supported by observations of enhanced CH_4 concentrations close to pycnocline and in the gas flare (25 nmol L^{-1}, Fig. 10). The dissolved CH_4 appears to be significantly diluted as the isotopic signature of the CH_4 released from the seafloor (−60‰ VPDB) is not identifiable anymore (−39.71‰ to −43.55‰ VPDB, red dots in Fig. 8A). Using the mean atmospheric methane concentration from June 2005 in this area of 1.903 ppm (Ocean Station ZEP: http://www.esrl.noaa.gov/gmd/ccgg/iadv/, at 78°54.6 N, 11°53.4 E) and the ambient values measured by CTD 34, the equilibrium methane concentration at the sea surface is 3.1 nmol L^{-1} according to Wiesenburg and Guinasso (1979). Consequently, the measured surface methane concentrations (Layer I) between 7.15 and 11.3 nmol L^{-1} indicate a saturation of 230–360%. Nevertheless, the amount of seafloor-released CH_4 in the water column as well as the atmospheric efflux could not been estimated and need to be verified by future works.

6. Summary and conclusions

Hydroacoustic flare imaging measurements revealed 10 active gas flares confirming previous measurements and indicating the continuity of these gas flares. This is in accordance with studies by Westbrook et al. (2009). It is important to consider that the amount of gas ebullition into the water column often varies with time. Several of the most intensively studied gas seeps (Greinert, 2008; Leifer and Boles, 2005; Schneider von Deimling et al., 2010) exhibited a pulsating behaviour, with periods of activity of several minutes or vigorous ebullitions. Therefore, long-term measurements are necessary to quantify the amount of CH_4 emissions from this gas ebullition area.

In close vicinity of these active seeps, a distinct plume very close to the seabed of strongly elevated methane concentration (up to 540 nmol L^{-1}) was identified by our high tempo-spatial measurements. The data revealed a strong decrease of methane concentrations within 20 m above the seafloor which indicates a fast dissolution of gas bubbles and/or diffusion from the sediment.

Even though some gas flares were observed rising up to 50 m water depth and higher in this region, the dissolved methane plume appears to be trapped by a pycnocline 20 m above the seafloor hindering the vertical transport and favoring the horizontal transport. Microbial methane oxidation rate measurements indicate elevated rates in the water 20 m above seafloor compared to the upper water column, which suggests ongoing microbial oxidation while the CH_4 load is transported with the current northwards in the same density layer. These results indicate that bubble transport can be excluded as a direct pathway of seafloor-released CH_4 to the atmosphere in the study area during the time of measurement.

However, during winter ice formation and resulting brine release leads to convective mixing down to the seafloor (supported by unpublished long term observations by A. Beszczynska-Möller). Summer stratification breaks down and vertical transport of CH_4 from Layer III is not limited anymore and can reach the sea surface. This seasonality of potential methane pathways is limited to high latitude regions and has been so far not considered in any budgets calculations such as the source calculation of atmospheric methane in higher latitudes by Fisher et al. (2011).

Acknowledgement

The authors thank the captain and the crew of *R/V Heincke* for their assistance during the cruise. We are indebted to Roi Martinez for the GIS support. We also thank Aysel Sorensen for helpful comments on the manuscript. Furthermore, we are grateful to Ingrid Stimac and Jennifer Ciomber for the help in the laboratory and to Ludmila Baumann for performing analyses during cruises.

References

Bell, R.J., Short, R.T., Amerom, F.H.W.v., Byrne, R.H., 2007. Calibration of an in situ membrane inlet mass spectrometer for measurements of dissolved gases and volatile organics in seawater. Environmental Science and Technology 41, 8123–8128.

Biastoch, A., Treude, T., Rupke, L.H., Riebesell, U., Roth, C., Burwicz, E.B., Park, W., Latif, M., Boning, C.W., Madec, G., Wallmann, K., 2011. Rising Arctic Ocean temperatures cause gas hydrate destabilization and ocean acidification. Geophysical Research Letters 38, L08602, http://dx.doi.org/10.1029/2011GL047222.

Buffett, B., Archer, D., 2004. Global inventory of methane clathrate: sensitivity to changes in the deep ocean. Earth and Planetary Science Letters 227, 185–199.

Cisewski, B., Budeus, G., Krause, G., 2003. Absolute transport estimates of total and individual water masses in the northern Greenland Sea derived from hydrographic and acoustic Doppler current profiler measurements. Journal of Geophysical Research-Oceans 108, 3298, http://dx.doi.org/10.1029/2002JC001530, C9.

Craig, H., 1957. Isotopic standards for carbon and oxygen and correction factors for mass-spectrometric analysis of carbon dioxide. Geochimica et Cosmochimica Acta 12, 133–149.

Damm, E., Mackensen, A., Budéus, G., Faber, E., Hanfland, C., 2005. Pathways of methane in seawater: plume spreading in an Arctic shelf environment (SW-Spitsbergen). Continental Shelf Research 25, 1453–1472.

Etiope, G., 2004. New directions: GEM – Geologic emissions of methane, the missing source in the atmospheric methane budget. Atmospheric Environment 38, 3099–3100.

Etiope, G., Klusman, R.W., 2002. Geologic emissions of methane to the atmosphere. Chemosphere 49, 777–789.

Faure, G., 1986. Principles of Isotope Geochemistry. John Wiley and Sons, New York. (Chapters 6, 8).

Felden, J., Wenzhofer, F., Feseker, T., Boetius, A., 2010. Transport and consumption of oxygen and methane in different habitats of the Hakon Mosby Mud Volcano (HMMV). Limnology and Oceanography 55, 2366–2380.

Fischer, P.J., 1978. Natural gas and oil seeps, Santa Barbara Basin, California. In: Fischer, P.J. (Ed.), California Offshore Gas, Oil, and Tar Seeps. California State Lands Commission, Sacramento, California, pp. 1–62.

Fisher, R.E., Sriskantharajah, S., Lowry, D., Lanoiselle, M., Fowler, C.M.R., James, R.H., Hermansen, O., Myhre, C.L., Stohl, A., Greinert, J., Nisbet-Jones, P.B.R., Mienert, J., Nisbet, E.G., 2011. Arctic methane sources: isotopic evidence for atmospheric inputs. Geophysical Research Letters 38, L21803, http://dx.doi.org/10.1029/2011GL049319.

Gentz, T., Schlüter, M., 2012. Underwater cryotrap-membrane inlet system (CT-MIS) for improved in situ analysis of gases. Limnology and Oceanography: Methods 10, 317–328.

Greinert, J., 2008. Monitoring temporal variability of bubble release at seeps: the hydroacoustic swath system GasQuant. Journal of Geophysical Research-Oceans 113, C07048, http://dx.doi.org/10.1029/2007JC004704.

Hovland, M., 2007. Discovery of prolific natural methane seeps at Gullfaks, northern North Sea. Geo-Marine Letters 27, 197–201.

Hovland, M., Judd, A.G., Burke, R.A., 1993. The global flux of methane from shallow submarine sediments. Chemosphere 26, 559–578.

Hovland, M., Sommerville, J.H., 1985. Characteristics of two natural gas seepages in the North Sea. Marine and Petroleum Geology 2, 319–326.

Hustoft, S., Dugan, B., Mienert, J., 2009. Effects of rapid sedimentation on developing the Nyegga pockmark field: constraints from hydrological modeling and 3-D seismic data, offshore mid-Norway. Geochemistry Geophysics Geosystems 10, Q06012, http://dx.doi.org/10.1029/2009GC002409.

Intergovernmental Panel on Climate Change, 2007. IPCC Fourth Assessment Report (AR4). Working Group 1, The Physical Science Basis.

Jerosch, K., Schlüter, M., Foucher, J.P., Allais, A.G., Klages, M., Edy, C., 2007. Spatial distribution of mud flows, chemoautotrophic communities, and biogeochemical habitats at Hakon Mosby Mud Volcano. Marine Geology 243, 1–17.

Judd, A.G., Davies, G., Wilson, J., Holmes, R., Baron, G., Bryden, I., 1997. Contributions to atmospheric methane by natural seepages on the UK continental shelf. Marine Geology 137, 165–189.

Judd, A.G., Hovland, M., 2007. Seabed Fluid Flow: The Impact on Geology, Biology and the Marine Environment. Cambridge University Press.

Jung, W.Y., Vogt, P.R., 2004. Effects of bottom water warming and sea level rise on Holocene hydrate dissociation and mass wasting along the Norwegian-Barents Continental Margin. Journal of Geophysical Research-Solid Earth 109, B06104, http://dx.doi.org/10.1029/2003JB002738.

Kampbell, D.H., Wilson, J.T., Vandegrift, S.A., 1989. Dissolved-oxygen and methane in water by a Gc headspace equilibration technique. International Journal of Environmental Analytical Chemistry 36, 249–257.

Kessler, J.D., Valentine, D.L., Redmond, M.C., Du, M.R., Chan, E.W., Mendes, S.D., Quiroz, E.W., Villanueva, C.J., Shusta, S.S., Werra, L.M., Yvon-Lewis, S.A., Weber, T.C., 2011. A persistent oxygen anomaly reveals the fate of spilled methane in the deep Gulf of Mexico. Science 331, 312–315.

Knies, J., Damm, E., Gutt, J., Mann, U., Pinturier, L., 2004. Near-surface hydrocarbon anomalies in shelf sediments off Spitsbergen: evidences for past seepages. Geochemistry Geophysics Geosystems 5, Q06003, http://dx.doi.org/10.1029/2003GC000687.

Kvenvolden, K.A., Rogers, B.W., 2005. Gaia's breath – global methane exhalations. Marine and Petroleum Geology 22, 579–590.

Lammers, S., Suess, E., 1994. An improved head-space analysis method for methane in seawater. Marine Chemistry 47, 115–125.

Landvik, J.Y., Ingolfsson, O., Mienert, J., Lehman, S.J., Solheim, A., Elverhoi, A., Ottesen, D., 2005. Rethinking Late Weichselian ice-sheet dynamics in coastal NW Svalbard. Boreas 34, 7–24.

Leifer, I., Boles, J., 2005. Measurement of marine hydrocarbon seep flow through fractured rock and unconsolidated sediment. Marine and Petroleum Geology 22, 551–568.

Leifer, I., Clark, J., 2002. Modeling trace gases in hydrocarbon seep bubbles. Application to marine hydrocarbon seeps in the Santa Barbara Channel. Geologiya i Geofizika 43, 613–621.

Leifer, I., Patro, R.K., 2002. The bubble mechanism for methane transport from the shallow sea bed to the surface: a review and sensitivity study. Continental Shelf Research 22 (16), 2409–2428.

Leifer, I., Judd, A.G., 2002. Oceanic methane layers: the hydrocarbon seep bubble deposition hypothesis. Terra Nova 14, 417–424.

Limonov, A.F., van Weering, T.C.E., Kenyon, N.H., Ivanov, M.K., Meisner, L.B., 1997. Seabed morphology and gas venting in the Black Sea mudvolcano area: observations with the MAK-1 deep-tow sidescan sonar and bottom profiler. Marine Geology 137, 121–136.

Mau, S., Heintz, M.B., Valentine, D.L., 2012. Quantification of CH_4 loss and transport in dissolved plumes of the Santa Barbara Channel, California. Continental Shelf Research 32, 110–120.

McGinnis, D.F., Schmidt, M., DelSontro, T.S., Themann, S, Rovelli, L., Reitz, A., Linke, P., 2011. Discovery of a natural CO_2 seep in the German North Sea: implications for shallow dissolved gas and seep detection. Journal of Geophysical Research-Oceans 116, C03013, http://dx.doi.org/10.1029/2010JC006557.

McGinnis, D.F., Greinert, J., Artemov, Y., Beaubien, S.E., Wüst, A., 2006. Fate of rising methane bubbles in stratified waters: how much methane reaches the atmosphere? Journal of Geophysical Research-Oceans 111, C09007, http://dx.doi.org/10.1029/2005JC003183.

Mienert, J., Vanneste, M., Bunz, S., Andreassen, K., Haflidason, H., Sejrup, H.P., 2005. Ocean warming and gas hydrate stability on the mid-Norwegian margin at the Storegga Slide. Marine and Petroleum Geology 22, 233–244.

Piechura, J., Beszczynska-Moller, A., Osinski, R., 2001. Volume, heat and salt transport by the West Spitsbergen Current. Polar Research 20, 233–240.

Rajan, A., Mienert, J., Bünz, S., 2012. Acoustic evidence for a gas migration and release system in Arctic glaciated continental margins offshore NW-Svalbard. Marine and Petroleum Geology 32, 36–49.

Rehder, G., Keir, R.S., Suess, E., Rhein, M., 1999. Methane in the northern Atlantic controlled by microbial oxidation and atmospheric history. Geophysical Research Letters 26, 587–590.

Saloranta, T.M., Svendsen, H., 2001. Across the Arctic front west of Spitsbergen: high-resolution CTD sections from 1998–2000. Polar Research 20, 177–184.

Sauter, E.J., Muyakshin, S.I., Charlou, J.L., Schlüter, M., Boetius, A., Jerosch, K., Damm, E., Foucher, J.P., Klages, M., 2006. Methane discharge from a deep-sea submarine mud volcano into the upper water column by gas hydrate-coated methane bubbles. Earth and Planetary Science Letters 243, 354–365.

Schauer, U., Fahrbach, E., Osterhus, S., Rohardt, G., 2004. Arctic warming through the Fram Strait: oceanic heat transport from 3 years of measurements. Journal of Geophysical Research-Oceans 109, C06026, http://dx.doi.org/10.1029/2003JC001823.

Schlüter, M., Gentz, T., 2008. Application of membrane inlet mass spectrometry for online and in situ analysis of methane in aquatic environments. Journal of the American Society for Mass Spectrometry 19, 1395–1402.

Schmale, O., Schneider von Deimling, J., Gülzow, W., Nausch, G., Waniek, J.J., Rehder, G., 2010. Distribution of methane in the water column of the Baltic Sea. Geophysical Research Letters 37 (12), L12604, http://dx.doi.org/10.1029/2010GL043115.

Schmitt, M., Faber, E., Botz, R., Stoffers, P., 1991. Extraction of methane from seawater using ultrasonic vacuum degassing. Analytical Chemistry 63, 529–532.

Schneider von Deimling, J., Greinert, J., Chapman, N.R., Rabbel, W., Linke, P., 2010. Acoustic imaging of natural gas seepage in the North Sea: sensing bubbles controlled by variable currents. Limnology and Oceanography: Methods 8, 155–171.

Schneider von Deimling, J., Rehder, G., Greinert, J., McGinnis, D.F., Boetius, A., Linke, P., 2011. Quantification of seep-related methane gas emissions at Tommeliten, North Sea. Continental Shelf Research 31, 867–878.

Shakhova, N., Semiletov, I., Salyuk, A., Yusupov, V., Kosmach, D., Gustafsson, Ö., 2010. Extensive methane venting to the atmosphere from sediments of the East Siberian Arctic shelf. Science 327, 1246–1250.

Shindell, D.T., Faluvegi, G., Koch, D.M., Schmidt, G.A., Unger, N., Bauer, S.E., 2009. Improved attribution of climate forcing to emissions. Science 326, 716–718.

Short, R.T., Fries, D.P., Kerr, M.L., Lembke, C.E., Toler, S.K., Wenner, P.G., Byrne, R.H., 2001. Underwater mass spectrometers for in situ chemical analysis of the hydrosphere. Journal of the American Society for Mass Spectrometry 12, 676–682.

Short, R.T., Fries, D.P., Toler, S.K., Lembke, C.E., Byrne, R.H., 1999. Development of an underwater mass-spectrometry system for in situ chemical analysis. Measurement Science and Technology 10, 1195–1201.

Slubowska-Wodengen, M., Rasmussen, T.L., Koc, N., Klitgaard-Kristensen, D., Nilsen, F., Solheim, A., 2007. Advection of Atlantic Water to the western and northern Svalbard shelf since 17,500 cal yr BP. Quaternary Science Reviews 26, 463–478.

Solomon, E.A., Kastner, M., MacDonald, I.R., Leifer, I., 2009. Considerable methane fluxes to the atmosphere from hydrocarbon seeps in the Gulf of Mexico. Nature Geoscience 2 (8), 561–565.

Tverberg, V., Nost, O.A., 2009. Eddy overturning across a shelf edge front: Kongsfjorden, west Spitsbergen. Journal of Geophysical Research-Oceans 114, C04024, http://dx.doi.org/10.1029/2008JC005106.

Valentine, D.L., Blanton, D.C., Reeburgh, W.S., Kastner, M., 2001. Water column methane oxidation adjacent to an area of active hydrate dissociation, Eel River Basin. Geochimica et Cosmochimica Acta 65, 2633–2640.

Walczowski, W., Piechura, J., Osinski, R., Wieczorek, P., 2005. The West Spitsbergen Current volume and heat transport from synoptic observations in summer. Deep-Sea Research Part I 52, 1374–1391.

Westbrook, G.K., Chand, S., Rossi, G., Long, C., Bunz, S., Camerlenghi, A., Carcione, J.M., Dean, S., Foucher, J.P., Flueh, E., Gei, D., Haacke, R.R., Madrussani, G., Mienert, J., Minshull, T.A., Nouze, H., Peacock, S., Reston, T.J., Vanneste, M., Zillmer, M., 2008. Estimation of gas hydrate concentration from multi-component seismic data at sites on the continental margins of NW Svalbard and the Storegga region of Norway. Marine and Petroleum Geology 25, 744–758.

Westbrook, G.K., Thatcher, K.E., Rohling, E.J., Piotrowski, A.M., Palike, H., Osborne, A.H., Nisbet, E.G., Minshull, T.A., Lanoiselle, M., James, R.H., Huhnerbach, V., Green, D., Fisher, R.E., Crocker, A.J., Chabert, A., Bolton, C., Beszczynska-Moller, A., Berndt, C., Aquilina, A., 2009. Escape of methane gas from the seabed along the West Spitsbergen continental margin. Geophysical Research Letters 36, L15608, http://dx.doi.org/10.1029/2009GL039191.

Wiesenburg, D.A., Guinasso, N.L., 1979. Equilibrium solubilities of methane, carbon-monoxide, and hydrogen in water and sea-water. Journal of Chemical and Engineering Data 24, 356–360.